

# Prediction of Mechanical Shaft Failures due to Pulsating Torques of Variable Frequency Drives

Joseph Song-Manguelle, *Senior Member, IEEE*, Stefan Schröder, *Member, IEEE*, Tobias Geyer, *Member, IEEE*, Gabriel Ekemb and Jean-Maurice Nyobe-Yome

**Abstract**—Mechanical damage of rotating shafts has been reported for several years from various high-power applications. This paper shows that the variable frequency drive incorporated in a rotating shaft is one of the main root causes of mechanical shaft failures. Simple analytical relationships show that the frequencies of the motor airgap torque have a more significant impact on the mechanical shaft failure than their magnitudes. Effects of mechanical damping are analytically derived and analyzed.

Motor airgap torque is successfully reconstructed using only the motor's voltage and current, thus avoiding torque sensors, which are subject to failure and errors. Simple relationships between frequencies of current harmonics and frequencies of motor pulsating torques are proposed. For pulse width modulated inverters (two and multi-level), possible drive operating points that might excite the shaft's eigenmodes are predicted.

Simulation results of four interleaved three-level neutral-point-clamped converters are analyzed for validation purposes. Experimental tests up to 35 MW are performed on a compressor test bed. The presented results confirm the accuracy of the proposed approach, which is particularly valuable for multi-megawatt drive applications.

**Index Terms**—Pulsating Torque, Torque Harmonics, Torsional Vibration, Mechanical resonance, Medium-voltage, Multi-level inverter, PWM, Oil and Gas, LNG, Mining, Cement.

## I. INTRODUCTION

For the past several years, the oil and gas industry has been increasingly moving from mechanical to electrical drive trains. Electrical motors, which were initially used to help the gas turbine start the compressor drive train, are now used as prime movers. Consequently, variable speed drive systems (VSDS) are becoming an important component of such large rotating shafts.

The trend to integrate VSDS into large rotating shafts has magnified the challenge to analytically understand and predict the rotor dynamics, VSDS behavior and shaft limits. However,

Paper 2009-IDC-382, presented at the 2009 Energy Conversion Conference and Exhibition, San Jose, CA, USA, September 20-24, and approved for publication in the IEEE TRANSACTIONS ON INDUSTRY APPLICATIONS by the Industrial Drives Committee of the IEEE Industry Applications Society. Manuscript submitted for review November 2, 2009 and released for publication February 11, 2010.

J. Song-Manguelle was with GE Global Research, Munich, Germany and GE Oil and Gas, Le Creusot, France. He is currently with GE Global Research, Niskayuna, NY, USA, joseph.song@ieee.org

S. Schröder is with GE Global Research, Munich, Germany.

T. Geyer was with GE Global Research, Munich Germany; he is currently with The University of Auckland, New Zealand

G. Ekemb is with ENSET, the University of Douala, Cameroon.

J.M. Nyobe-Yome is with ENSET, the University of Douala, Cameroon and with the University of Quebec in Abitibi-Temiscamingue, Rouyn-Noranda, QC, J9X 5E4, Canada.

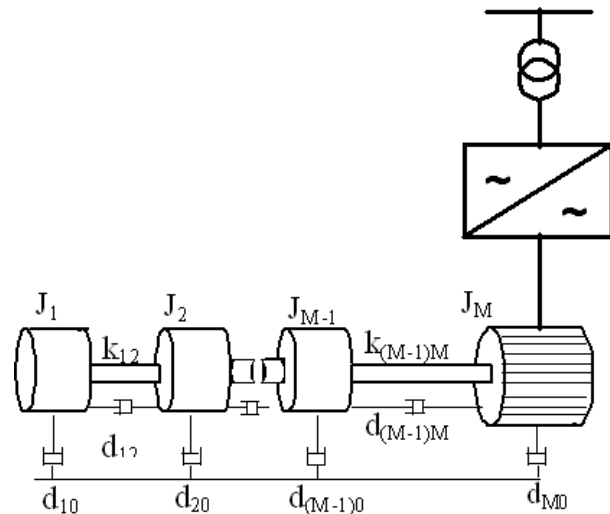


Fig. 1. General representation of a rotating shaft with integrated VSDS

several past investigations mainly focused on understanding VSDS issues related to its performance and its integration into an electrical network (grid side harmonic compliance with the IEEE 519 standard, etc.). On the motor side, issues related to current harmonic minimization or cancellation were also reported, as well as motor compatibility with the VSDS (common mode voltage, bearing currents, voltage spikes, etc.) [1]-[5]. With regards to the torque, investigations are usually limited to controlling its DC component. Dynamic airgap torque equations of the motor are insufficient to predict mechanical shaft failures.

Mechanical damages of rotating shafts were reported due to pulsating torques [6]-[8]. A modeling approach to better understand torsional resonances in drive trains was proposed in [9]. However, the propagation of the torque signal on the shaft is not analytically analyzed. Understanding the torque propagation may help to predict mechanical shaft failures.

Airgap torque harmonics generated by pulse width modulated (PWM) inverters were calculated in [10]. But the developed relationships do not show any clear link between current harmonic frequencies and the generated pulsating torque frequencies. Several techniques were investigated to reduce or cancel selected current harmonics. So far, the main target has been the reduction of low-order current harmonics and the improvement of the current's total harmonic distortion (THD), [11]. Yet, low-order torque harmonics might not be affected by canceling low-order current harmonics.

This paper explains how the drive's pulsating torque propa-

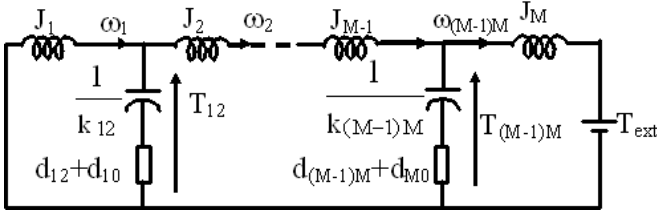


Fig. 2. Equivalent electrical circuit of a generalized shaft system

gates on a rotating shaft. It shows that mechanical shaft failure is mostly determined by the frequency of a drive's pulsating torque and not by its magnitude. A direct relationship between current harmonic frequencies and pulsating torque frequencies is proposed. Therefore all analytical developments performed in previous works to predict current harmonics of drives such as LCIs, two-level and multi-level PWM converters can be easily used to predict pulsating torque frequencies of variable speed drives.

Four three-level PWM neutral-point-clamped converters, which are connected in parallel, are investigated to validate the suggested relationships. The overall rating of the drive is 35 MW. The effect interleaving has on the current harmonics is analyzed and related to the torque harmonics. The design, performance and control strategy of that system have been previously described in [12], [13].

## II. ANALYSIS OF ROTATING SHAFT OSCILLATIONS

### A. Preliminary Considerations

A general representation of a rotating shaft system is shown in Fig. 1. Its phenomenological equivalent electrical circuit is shown in Fig. 2. According to [9], moments of inertia are equivalent to inductances, damping factors to resistances, inverse stiffnesses to capacitances. Angular velocities can be seen as currents and torques are equivalent to potential differences measured on the circuit against a common reference, as illustrated in Fig. 2.

An important outcome of this approach is that a rotating mechanical shaft can be analyzed in the same way as a simple *RLC* circuit. Based on Newton's second law, a polynomial differential equation can be established [14], that is valid for oscillations on electrical and mechanical systems and which can be solved analytically [15].

To simplify the exposition, this section is restricted to shaft systems with one inertia  $J$ , one damping coefficient  $D$  and one stiffness constant  $K$ . The shaft's angular position is denoted by  $\theta$  and an external torque  $T_{ext}$  is applied to the rotating mass. The system differential equation can be written as

$$\frac{d^2\theta}{dt^2} + 2n\frac{d\theta}{dt} + k^2\theta = f(t), \quad (1)$$

where  $n = D/(2J)$ ,  $k = \sqrt{K/J}$ ,  $f(t) = T_{ext}/J$ .

### B. Shaft Behavior with an Externally Applied Periodic Torque

This case is particularly interesting with regards to large motor drive applications, which are typically found in the mining, cement or oil and gas industry. Depending on the

drive's operating point and settings, the shaft is usually excited by a set of torque components at several frequencies. For simplicity, we assume that the externally applied torque is a sine wave such that  $f(t) = T_a \sin(\omega t)$ .

Assuming  $n \neq 0$  and  $n^2 < k^2$  such that  $k_1 = \sqrt{k^2 - n^2}$  is real, the solution of (1) is given by

$$\theta(t) = \theta_f(t) + \theta_F(t), \quad (2)$$

which has two terms. The first term  $\theta_f$  represents the free oscillation, while the second term  $\theta_F$  denotes the forced oscillation:

$$\theta_f(t) = Ae^{-nt} \sin(k_1 t + \sigma_f) \quad (3a)$$

$$\theta_F(t) = B \sin(\omega t + \sigma_F), \quad (3b)$$

with

$$A = \frac{B^2}{T_a} \sqrt{\left[ (2n^2 - k^2 + \omega^2) \frac{\omega}{k_1} \right]^2 + (2n\omega)^2}, \quad (4a)$$

$$B = \frac{T_a}{\sqrt{(k^2 - \omega^2)^2 + (2n\omega)^2}} \quad (4b)$$

$$\tan(\sigma_f) = \frac{2k_1\omega}{2n^2 - k^2 + \omega^2} \text{ and } \tan(\sigma_F) = -\frac{2n\omega}{k^2 - \omega^2}.$$

1) *Effect of damping factors*: If the system is not damped, i.e.  $n = 0$ , (3) reduces to

$$\theta_f(t) = \frac{T_a}{k^2 - \omega^2} \frac{\omega}{k} \sin(kt + \sigma_f) \quad (5a)$$

$$\theta_F(t) = \frac{T_a}{k^2 - \omega^2} \sin(\omega t + \sigma_F), \quad (5b)$$

where  $\tan(\sigma_f) = -\frac{2k\omega}{k^2 - \omega^2}$  and  $\sigma_F = 0$ .

The magnitude of the two components does not depend on time. Eq. 5 also shows that an externally applied force of high frequency has only a minor effect on the shaft, since the free and forced components become negligible ( $\theta_f \rightarrow 0, \theta_F \rightarrow 0$  if  $\omega \rightarrow \infty$ ).

2) *Long term shaft behavior*: For a larger  $t$  (3) indicates that the shaft's angular position depends only on the forced oscillations, since the damping factor reduces the effect of the free oscillation ( $e^{-nt} \rightarrow 0$  for  $t \rightarrow \infty$ ). In drive applications, this case usually occurs when the shaft is operating at a constant speed, or when the speed is slowly varying or drifting over time. Therefore, the forced oscillation can be written as

$$\theta_F(t) = \frac{T_a}{k^2 \sqrt{(1 - \lambda^2)^2 + (\lambda\gamma)^2}} \sin(\omega t + \sigma_F), \quad (6)$$

where  $\lambda = \omega/k$  and  $\gamma = 2n/k$ .  $\theta_F(t)$  reaches its maximum

$$\max_{\lambda}(\theta_F) = \frac{T_a}{k^2 \gamma \sqrt{1 - \gamma^2/4}} \quad (7)$$

at  $\lambda_0 = \sqrt{1 - \lambda^2/2}$ . This equation highlights that for an external force of low magnitude, the magnitude of the shaft oscillation can still reach huge values, if the forced frequency is very close to the shaft's natural (eigen) frequencies. Eq. 6 also shows that externally applied forces of high frequencies will have minor effects on the shaft oscillation, if they are located far away from the natural frequencies of the shaft.

In large shafts torsional modes are usually located at low frequencies. If, however, there are  $M$  dedicated rotor sections on the shaft, there will be  $M-1$  natural frequencies. Therefore, external high frequency oscillations located close to the highest natural frequency can still create a huge shaft oscillation.

3) *Shaft behavior without damping but with an externally applied periodic torque at the shaft's natural frequency:* Setting  $n = 0$  and  $\omega = k$  in (1) and solving the differential equation yields

$$\theta(t) = \frac{T_a}{2k} \left( \frac{1}{k} \sin(kt) - t \cos(kt) \right), \quad (8)$$

which has one component with the constant magnitude  $T_a/(2k^2)$  and another one with a magnitude linearly increasing with time, i.e.  $tT_a/(2k)$ , as shown in [9].

Therefore, any torque harmonic located near a shaft's natural frequency will create an oscillation whose magnitude increases indefinitely over time, potentially leading to accelerated fatigue or severe damage of the train, unless sufficiently damped.

### C. Possible sources of torsional stimulus

Large rotating machineries involving electrical machines are subject to diverse disturbances which can result in torque oscillations (externally applied torque  $T_{ext}$ ) applied to the shaft assembly and may stimulate twisting oscillations of the rotating shaft. Those stimulus forces can be classified in mechanical and electromagnetic kinds [16], [17].

Mechanical stimulus forces may be generated from structural irregularities such as static or dynamic unbalance rotating parts, asymmetrical mechanical parts, friction, loose of bearings, destruction of gear tooth, etc.

Electromagnetic stimulus forces are those created by electromagnetic phenomenon such as radial magnetic attraction between stator and rotor, magneto-motive forces (MMF) in the motor airgap which are influenced by the machine construction (slot in the stator or rotor). MMF are created by the voltage applied at the machine terminals.

For variable speed applications, the machine voltage is generated by a variable frequency drive (VFD). Several aspects and parameters of VFD operation are able to influence the machine voltages [18]-[20] (e.g. PWM strategy, motor/drive loads instability, inverter dead time, parasitic effects on the control, etc). They may influence the motor MMF, potentially leading to torsional oscillations. For simplicity, in this paper we assume that the externally applied forces to the shaft correspond to the machine airgap torque caused by the PWM strategy of VFD only.

Drive control and modulation strategies should thus avoid generating airgap torque harmonic components located near the shaft's natural frequencies. Based on our experience, large shafts can be excited with a pulsating torque magnitude as low as 0.65% of the nominal torque [21]. Certain operating points of the drive or transient behavior (change of the speed command) can create an externally applied torque component on the shaft at its natural frequency.

The main statements formulated in this section can be directly extended to a multi-rotor system as shown in Fig. 1. The

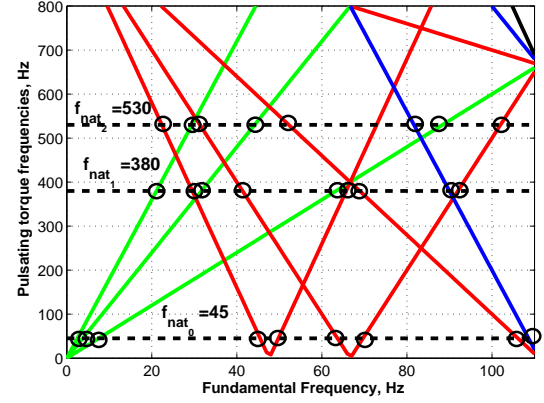


Fig. 3. Campbell diagram: fundamental frequencies that may excite torsional modes in the shaft. These frequencies are given by the intersections of pulsating torque frequencies with natural (eigen) frequencies of the shaft.

prediction of drive operating points that lead to the generation of torque harmonic components located at the shaft's natural frequencies is vital to avoid possible shaft damages.

### D. Basic Principle of Shaft Excitation with VFD

It's usually assumed that the natural frequencies of the rotating mechanical load are constant and do not depend on the system speed. It's also assumed that these frequencies are calculated with very high accuracy. Effects of the variability of the shaft's natural frequencies are analyzed in [10].

An electric machine coupled to a mechanical shaft generates a set of periodic torque components, which depend on the operating point of the machine – more specifically, they are defined by the fundamental frequency of the current flowing through the stator windings. The frequency of the stator currents depends on the topology, and on the control and modulation scheme used for the VSIS (Load Commutated Inverter and its number of pulses in the grid and motor sides, voltage source inverter and its modulation strategy, etc). Newton's differential equation given in Eq. 1 can be rewritten as follows:

$$\frac{d^2\theta}{dt^2} + 2n\frac{d\theta}{dt} + k^2\theta = T_0 + T_1 \sin(\omega_1 t) + T_2 \sin(\omega_2 t) + \dots \quad (9)$$

Here,  $T_0$  is the DC component of the airgap torque, which corresponds to the desired torque needed to drive the shaft.

It can be shown that the airgap torque frequencies  $f_1, f_2, \dots$  are linearly dependent on the machine's rotational speed, and thus depend on the stator current's fundamental frequency [10]. The eigenmode of the mechanical shaft gets excited if any of the airgap torque components is located sufficiently close to an eigenfrequency of the shaft. These locations are shown in Fig. 3.

## III. STATOR CURRENT HARMONICS AND PULSATING TORQUE FREQUENCIES IN PWM VSI

### A. Voltage Harmonics of PWM Drives

The harmonic spectrum of PWM converters is characterized by integer multiples of the fundamental frequency  $f_0$  and the

carrier frequency  $f_c$ . According to [22] each harmonic  $h_{mn}(t)$  can be written as

$$h_{mn}(t) = C_{mn} \cos(m(\omega_c t + \theta_c) + n(\omega_0 t + \theta_0) + \theta_{mn}), \quad (10)$$

where  $\omega_c = 2\pi f_c$  and  $\omega_0 = 2\pi f_0$ .

Here,  $\theta_c$  and  $\theta_0$  are the phase of the carrier and the fundamental, respectively;  $C_{mn}$  and  $\theta_{mn}$  are expressions depending on the modulation scheme;  $m$  and  $n$  are integer constants. Different combinations of  $m$  and  $n$  can result in the same harmonic frequency, especially when synchronous PWM is used. In the PWM voltage spectrum, the (geometric) sum of all harmonic components described by (10) is visible. According to [23], even values of  $m$  are paired with odd values of  $n$  and vice versa for 3-level phase disposition natural sampled PWM. All other combinations yield zero amplitudes of the corresponding harmonic. Practical modulator implementations based on space-vector PWM behave qualitatively similar to this.

An important conclusion from (10) is that the amplitude  $C_{mn}$  of a certain harmonic does not change if the phase of the fundamental and/or the carrier is changed. Under this condition, only the phase  $\theta_{h,mn}$  of the harmonic is changed according to

$$\theta_{h,mn} = m\theta_c + n\theta_0 + \theta_{mn}. \quad (11)$$

In a symmetrical 3-phase system, the three fundamental references have a phase shift  $\theta_0$  of  $0^\circ$ ,  $120^\circ$  and  $240^\circ$ , respectively. Hence, the phase shift of the resulting harmonic is  $0^\circ$ ,  $n \cdot 120^\circ$  and  $n \cdot 240^\circ$ , respectively. Depending on the value of  $n$  modulo 3, i.e. 0, 1 or 2, the corresponding harmonics form a zero, positive or negative sequence system. Since the star-point of electrical machines is typically not connected with the converter, the zero sequence voltages in the PWM pattern do not generate any machine current.

### B. Direct Relationship between Current and Torque Frequencies

To understand the resulting torque spectrum, it is instructive to transfer the harmonics from stationary to rotating coordinates. Here, positive and negative sequence harmonics behave differently. The former are reduced by one harmonic order, while the latter are increased by one.

To illustrate this, we consider sideband harmonics around even multiples of the carrier ( $m$ =even). These have, as stated above, sidebands with odd numbers, i.e.  $n = \pm 1, \pm 3, \pm 5, \pm 7$ , and so on. The zero-sequence harmonics do not generate any current, whereas the other harmonics generate sidebands at  $0, \pm 6, \dots$  in rotating coordinates, i.e. at even multiples of 3 (for  $m$ =even). Conversely, the sidebands for  $m$ =odd comprise odd multiples of 3, i.e.  $\pm 3, \pm 9$ , etc.

The torque can be expressed as a product of two currents in rotating coordinates. As long as these currents are dominated by large dc-components, the products of two harmonics can be neglected and the torque harmonic spectrum is similar to the current spectrum in rotating coordinates.

Let  $(x, y)$  be a short notation for the torque harmonic frequencies [10]

$$F_{xy, T_e} = |xf_c \pm yf_0| \quad (12)$$

and  $(m, n)$  denotes the current harmonic frequencies [23]

$$F_{mn, I_a} = |mf_c \pm nf_0|. \quad (13)$$

Based on the above statements and according to [10], the following relationship can then be stated: A torque harmonic component located at  $(x, y)$  is generated by the two current harmonics at  $(m, n)$ , where

$$\begin{aligned} m &= x \\ n &= y \pm 1. \end{aligned} \quad (14)$$

### C. Detailed Relationships between Torque and Current Harmonic Frequencies

- Baseband harmonics:

$$\begin{aligned} x &= 0 \\ y &= 6j, \forall j = 1, 2, 3, \dots \end{aligned} \quad (15)$$

Examples are given in Table I.

- Sidebands around even multiples of the carrier frequency:

$$\begin{aligned} x &= 2i, \forall i = 1, 2, 3, \dots \\ y &= 3(2j), \forall j = 0, 1, 2, \dots \end{aligned} \quad (16)$$

Examples are given in Table II.

- Sidebands around odd multiples of the carrier frequency:

$$\begin{aligned} x &= 2i + 1, \forall i = 0, 1, 2, \dots \\ y &= 3(2j + 1), \forall j = 0, 1, 2, \dots \end{aligned} \quad (17)$$

Examples are given in Table III.

$(x, y)$	$F_{xy, T_e}$	$F_{mn, I_a}$
(0, 6)	$6f_0$	$5f_0, 7f_0$
(0, 12)	$12f_0$	$11f_0, 13f_0$
(0, 18)	$18f_0$	$17f_0, 19f_0$

TABLE I  
BASEBAND TORQUE AND GENERATING CURRENT HARMONICS

$(x, y)$	$F_{xy, T_e}$	$F_{mn, I_a}$
(2, 0)	$2f_c$	$2f_c \pm f_0$
(2, 6)	$ 2f_c \pm 6f_0 $	$ 2f_c \pm 5f_0 ,  2f_c \pm 7f_0 $
(2, 12)	$ 2f_c \pm 12f_0 $	$ 2f_c \pm 11f_0 ,  2f_c \pm 13f_0 $
(4, 0)	$4f_c$	$4f_c \pm f_0$
(4, 6)	$ 4f_c \pm 6f_0 $	$ 4f_c \pm 5f_0 ,  4f_c \pm 7f_0 $
(4, 12)	$ 4f_c \pm 12f_0 $	$ 4f_c \pm 11f_0 ,  4f_c \pm 13f_0 $

TABLE II  
SIDE BAND TORQUE AND GENERATING CURRENT HARMONIC COMPONENTS FOR EVEN  $m$

The relationships proposed in this section show that, based on current harmonic frequencies, the pulsating torque frequencies can be predicted for a torsional analysis. For the

$(x, y)$	$F_{xy, T_e}$	$F_{mn, I_a}$
(1, 3)	$ f_c \pm 3f_0 $	$ f_c \pm 2f_0 ,  f_c \pm 4f_0 $
(1, 9)	$ f_c \pm 9f_0 $	$ f_c \pm 8f_0 ,  f_c \pm 10f_0 $
(3, 3)	$ 3f_c \pm 3f_0 $	$ 3f_c \pm 2f_0 ,  3f_c \pm 4f_0 $
(3, 9)	$ 3f_c \pm 9f_0 $	$ 3f_c \pm 8f_0 ,  3f_c \pm 10f_0 $

TABLE III  
SIDE BAND TORQUE AND GENERATING CURRENT HARMONIC  
COMPONENTS FOR ODD  $m$

integration of large PWM drives such as multi-level converters, pulsating torque frequencies can be predicted with good accuracy without too much of a mathematical effort. Such predictions can be established using the well accepted analytical expressions of voltage or current PWM converters [22], [23].

These results also show that current harmonic elimination techniques become more effective regarding the torque spectrum if the two current components that generate one specific torque harmonic are fully eliminated. Cancellation of only one current harmonic will reduce the magnitude of the torque component without fully eliminating it.

#### D. Current Harmonic Cancellation with Interleaving

In the interleaved system, each PWM unit uses the same fundamental and carrier frequencies but the phase of the carrier differs for each converter. By choosing the phases  $\theta_{c,i}$  for each converter  $i$ , certain classes of harmonics can be canceled. The harmonics of each thread are the same but phase shifted by  $m\theta_{c,i}$  according to (11). Considering a four-thread system and using the phases

$$\theta_{c,1} = 0, \theta_{c,2} = \frac{\pi}{4}, \theta_{c,3} = \frac{\pi}{2}, \theta_{c,4} = \frac{3\pi}{4}, \quad (18)$$

all current harmonics with  $m = 2, 4, 6, \dots$  (for all  $n$ , i.e. including their sidebands) are canceled and harmonics with  $m = 1, 3, 5, \dots$  are reduced but not canceled. Since  $m = x$ , all torque harmonics located at  $x = 2, 4, 6, \dots$  are thus completely removed.

#### E. Airgap Torque Reconstruction from the Machine Voltage and Current

Measuring directly the motor's airgap torque is generally not possible. Torque sensors mounted on the shaft may be used to measure the mechanical torque thus providing an approximative measurement of the airgap torque. However, the installation of such sensors is error prone and often not desired – particularly in environments where explosives are present, as in the case of Oil and Gas applications. Most importantly, torque sensors often have a limited bandwidth, which is typically in the range of a few hundred Hz.

Yet, electrical quantities such as the machine voltages and currents are routinely measured with high accuracy and high bandwidth, which can be in the order of several kHz. Therefore, it is not only convenient but also beneficial to reconstruct the airgap torque from electrical quantities, i.e. from the (three-phase) line to line machine voltage and the (three-phase) machine phase current.

The method to reconstruct the airgap torque consists of three steps:

- 1) Transform the three-phase machine voltage ( $u_{abc}$ ) and current ( $i_{abc}$ ) into the stationary  $\alpha\beta 0$  coordinate system using the peak invariant transformation as shown in Eq. 19; where  $i_{s\alpha}$  and  $i_{s\beta}$  denote the machine's stator current in  $\alpha$  and  $\beta$ , respectively. Details of such transformation are provided in [14], [24].

$$u_{s\alpha\beta 0} = M * u_{abc} \quad \text{and} \quad i_{s\alpha\beta 0} = M * i_{abc} \quad (19a)$$

$$\text{with } M = \frac{2}{3} \begin{pmatrix} 1 & -\frac{1}{2} & -\frac{1}{2} \\ 0 & \frac{\sqrt{3}}{2} & \frac{\sqrt{3}}{2} \\ \frac{1}{2} & \frac{1}{2} & \frac{1}{2} \end{pmatrix}. \quad (19b)$$

- 2) Compute the integral over time of the machine voltage in  $\alpha\beta$ . To obtain the stator flux linkage in  $\alpha\beta$ , i.e.  $\psi_{s\alpha}$  and  $\psi_{s\beta}$ , any offset and linear trend is removed from the integral. Note that, in general, an offset is present in the integral since – for simplicity – the integral starts from zero as initial value. A linear trend might result for example from offsets in the voltage measurements. Yet, as will be seen in the experimental part, since the method includes an integration step, this approach remains sensitive to low-frequency measurement noise both in the amplitude and the phase.
- 3) Assuming SI quantities, the airgap torque is computed using

$$T_e = \frac{3P}{2} (\psi_{s\alpha} i_{s\beta} - \psi_{s\beta} i_{s\alpha}), \quad (20)$$

where the factor  $3/2$  stems from the usage of the peak invariant transformation and  $P$  denotes the number of poles. A similar torque equation can be derived when the electrical quantities are given in per unit. Expressions of airgap torque of synchronous machine in different reference frames are given in [24].

The torque reconstruction method suggested in this section is mainly valuable for a high-power VSDS running in high-power operation range, where the machine losses are relatively low compare to its absorbed power. Stator losses have been neglected, therefore the related error in reconstructed torque is small since the relative losses of the machine are relatively low. For low-speed operating region, a flux estimation method developed for sensorless control can be adopted, taking into account stator resistance value, which is sensitive to stator current frequency and winding temperature [25].

However the machine characteristics are reflected in the measured machine current. These characteristics may naturally include nonlinear effects such as saturation, the skin effect, stator resistor thermal drift. As a consequence, error in reconstructed torque using measured machine's voltage and current which is due to flux estimation error is reduced.

## IV. THEORETICAL VALIDATION

### A. VSDS Topology and Control

To validate the correlation between current and torque harmonics described in the previous sections, the system shown in Fig. 4 is considered. Four three-level neutral point clamped (NPC) converters based on IGCTs are connected in parallel via external coupling inductances. Each NPC converter is

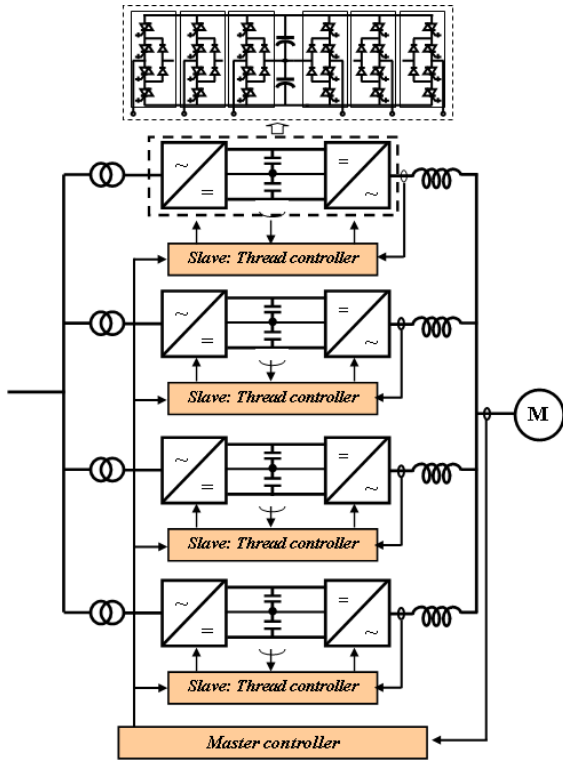


Fig. 4. Validation system: VSDS topology and control

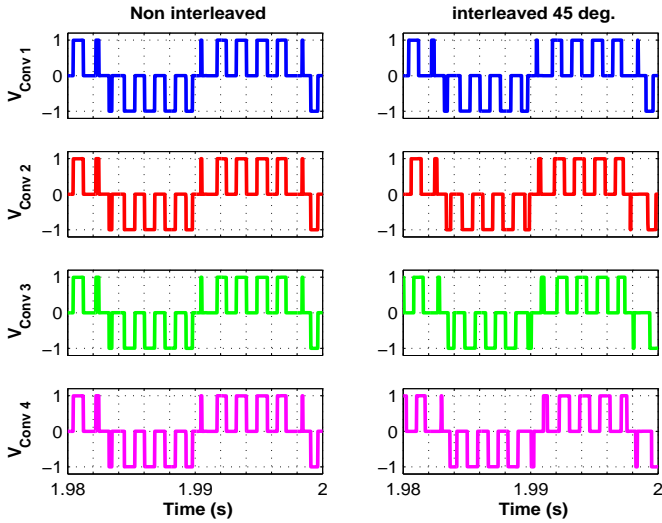


Fig. 5. Converter voltages of the 4 threads for  $f_c = 625$  Hz and  $f_0 = 65$  Hz

connected to a 33 kV grid via a step-down transformer (33 kV / 3 kV). The machine is a synchronous machine, with a nominal speed of 3000 rpm and rated at 35 MW. A detailed description of this VSDS can be found in [13].

The four threads can operate with synchronous commands. Then, the system behaves like a single high-power three-phase three-level NPC converter. Alternatively, the PWM signals of the converters can be interleaved by phase shifting the carrier angle by  $45^\circ$  as shown in Fig. 5.

For the theoretical validation, the system was simulated in SABER. For this, the active front ends were neglected and

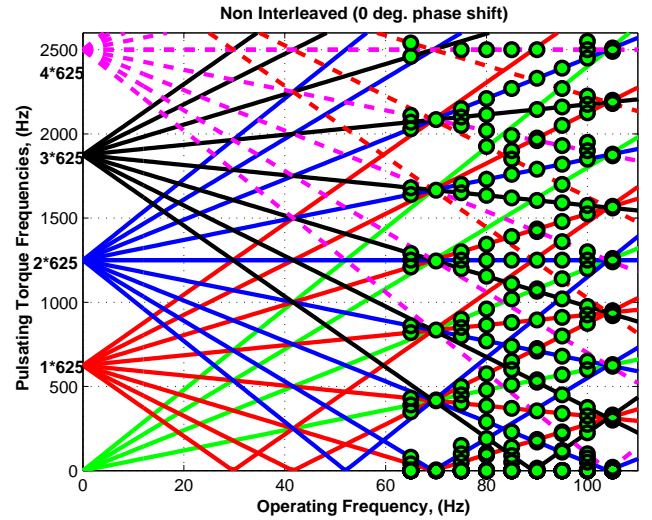


Fig. 6. Campbell diagram: non-interleaved case with  $f_c = 625$  Hz when varying  $f_0$  from 0 to 105 Hz. Lines are prediction and 'o' are simulation results

replaced by constant voltage sources. For the experimental validation, a full-scale VSDS rated at 35 MW was built and tested extensively [13].

A total of 35 cases was simulated at different operating points and different carrier frequencies. The torque spectrum of the motor was calculated using a *fast fourier transformation* (FFT) with a 5 Hz resolution. The window length of the FFT was selected to be an integer multiple of the fundamental period.

The combination of carrier and fundamental frequencies were always chosen in such way that the expected torque harmonics according to Eq. 12, would be integer multiple of 5 Hz only. Smaller resolution may be chosen, but required longer simulation time for such a complex system. Data was recorded once the system had reached its steady state. The obtained results are analyzed and summarized in the next sections.

### B. Theoretical Validation: 4-Thread Non-Interleaved System

1) *Predicted and simulated torque harmonics*: The motor's fundamental frequency is varied from 65 Hz to 105 Hz with a step size of 5 Hz. For many oil and gas applications, the operating range is within 65 – 105% of the nominal frequency. In this case, the nominal frequency is 100 Hz. The torque harmonics are extracted and plotted in the same Campbell diagram as the predicted torque harmonics, as shown in Fig. 6. An excellent correlation between the predicted and the simulated pulsating torque frequencies can be observed.

2) *Correlation between current and torque harmonics*: The first column of Fig. 5 shows the non-interleaved output voltages (phase to dc-midpoint) of each of the four converters, when using the carrier frequency  $f_c = 625$  Hz at the operating point given by  $f_0 = 65$  Hz. The voltages seen by the motor after the coupling inductances, the motor currents and the airgap torque are shown in Fig. 7. The spectra of the motor

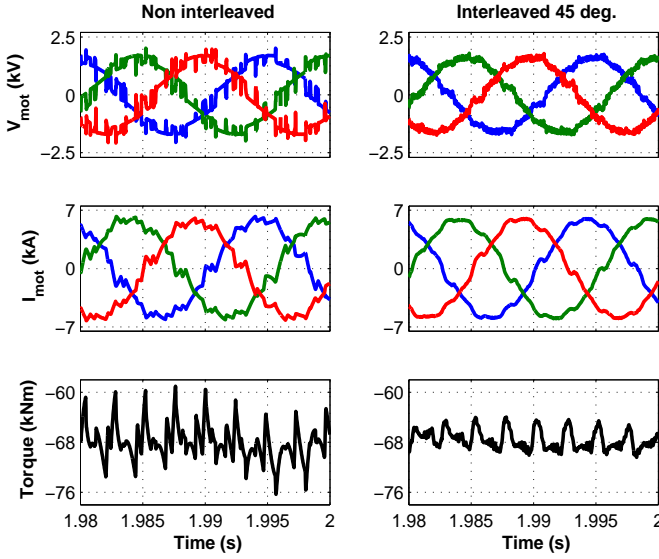


Fig. 7. Motor voltages, currents and torque for  $f_c = 625$  Hz and  $f_0 = 65$  Hz

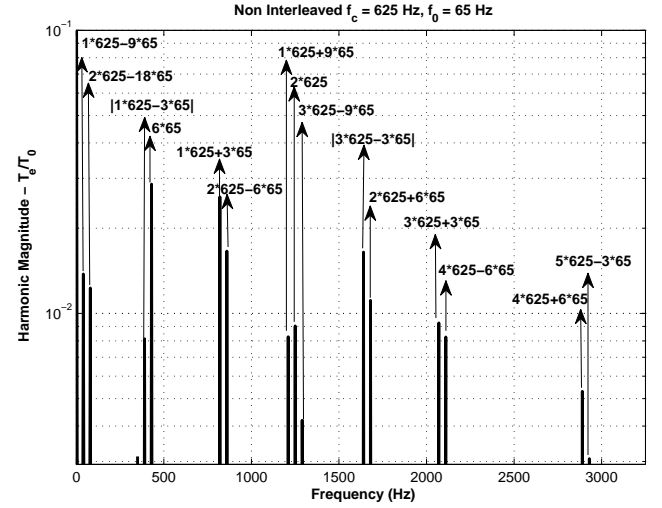


Fig. 9. Non-interleaved torque spectrum,  $f_c = 625$  Hz,  $f_0 = 65$  Hz

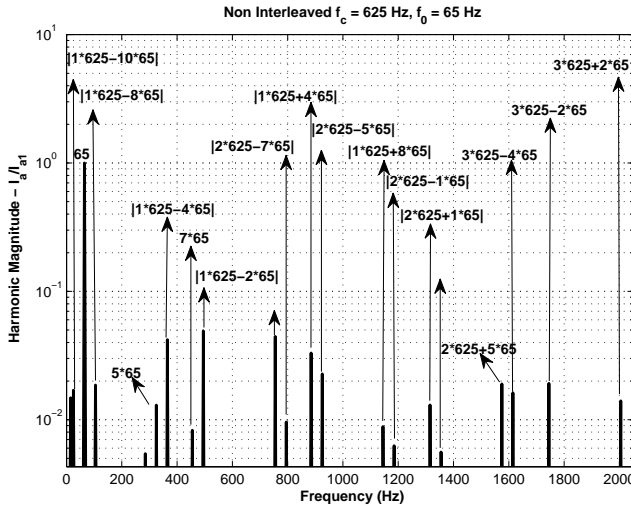


Fig. 8. Non-interleaved current spectrum,  $f_c = 625$  Hz,  $f_0 = 65$  Hz

current and airgap torque are illustrated in Figs. 8 and 9, showing the exact values of the harmonic frequencies.

The results show an excellent correlation between calculation (prediction) and simulation. Hereafter, a few examples are given that can be also found in Tables I to III:

- The torque component located at 0 Hz (dc-component) is created by the current component located at  $|(0 \pm 1) \cdot 65|$  Hz (fundamental current).
- The torque component located at  $|1 \cdot 625 - 9 \cdot 65|$  Hz (see Fig. 9) is created by the two current components located at  $|1 \cdot 625 - (9 \pm 1) \cdot 65|$  Hz (see Fig. 8).
- The torque component located at  $6 \cdot 65$  Hz is created by the two current components located at  $(6 \pm 1) \cdot 65$  Hz.
- The torque component located at  $|2 \cdot 625 - 6 \cdot 65|$  Hz (see Fig. 9) is created by the two current components located at  $|2 \cdot 625 - (6 \pm 1) \cdot 65|$  Hz (see Fig. 8), etc.

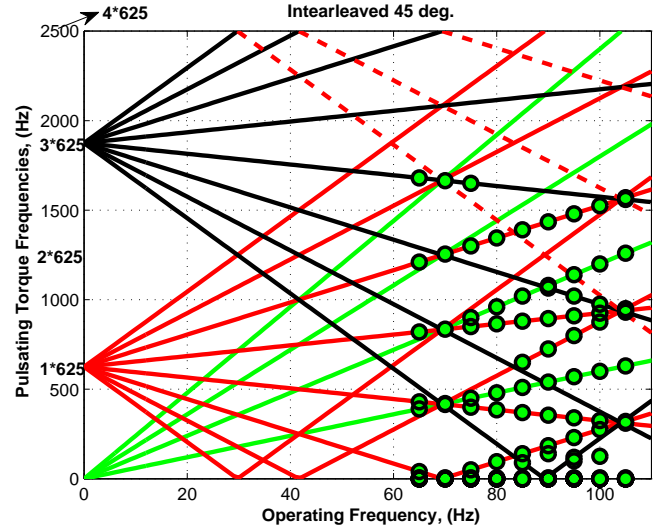


Fig. 10. Campbell diagram: interleaved case with  $45^\circ$  carrier phase shift and  $f_c = 625$  Hz when varying  $f_0$  from 0 to 105 Hz. Lines are prediction and 'o' are simulation results

### C. Theoretical Validation: 4-Thread $45^\circ$ Interleaved System

1) *Predicted and simulated torque harmonics:* Simulations were performed accordingly for the interleaved case, where the PWM carriers were phase-shifted by  $45^\circ$ . The second column of Fig. 5 shows the simulated phase to dc-midpoint voltage waveforms of each converter. The three-phase voltages seen by the motor, as well as the stator currents and the motor torque are shown in the second column of Fig. 7.

In Fig. 10 the predicted torque harmonic frequencies are plotted along with the simulated ones with a 5 Hz resolution. Also in this case, an excellent correlation between the predictions and the simulations can be stated. It can be seen that torque harmonics located at even multiple of the carrier frequency are canceled, as predicted in the previous section, due to current harmonic cancellation.

2) *Correlation between current and torque harmonics:* The spectra of the motor current and airgap torque are depicted in

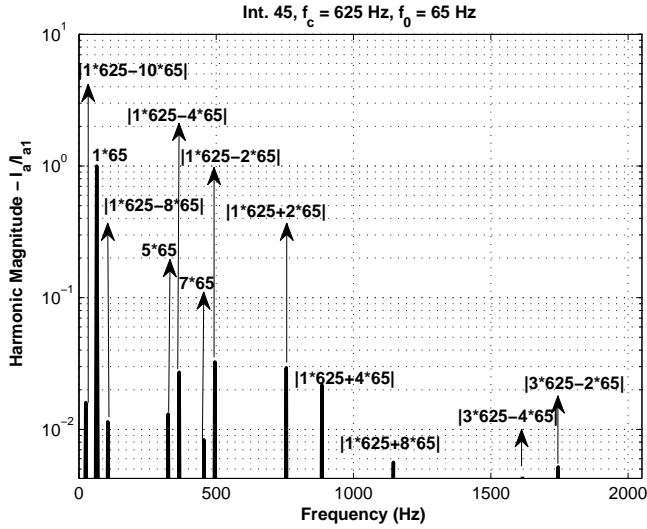


Fig. 11.  $45^\circ$  interleaved current spectrum,  $f_c = 625$  Hz,  $f_0 = 65$  Hz

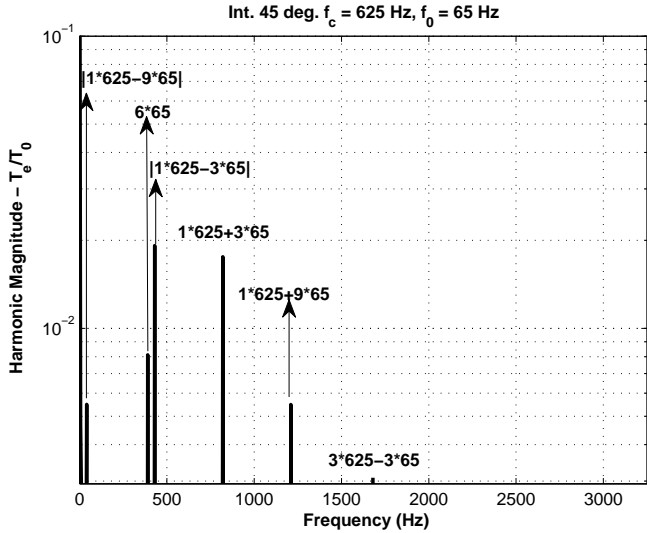


Fig. 12.  $45^\circ$  interleaved torque spectrum,  $f_c = 625$  Hz,  $f_0 = 65$  Hz

Fig. 11 and Fig. 12 showing the exact values of the harmonic frequencies. The results indicate an excellent correlation between predictions and simulations.

#### D. Theoretical Validation: Airgap Torque Reconstruction from the Machine Voltage and Current

The previous section's Saber simulations of the VSFS provide a good opportunity to verify the torque reconstruction methodology introduced previously. For this, we consider the following setup: Carrier frequency  $f_c = 625$  Hz, fundamental frequency  $f_0 = 100$  Hz and no interleaving. This leads to the simulated airgap torque shown as a dashed line in Fig. 13. Using only the simulated stator current and machine voltage, the method described in Section III-E can be used to reconstruct the airgap torque. The reconstructed torque is shown as a straight line (on top of the dashed line denoting the simulated torque) in Fig. 13. As this figure indicates, a close

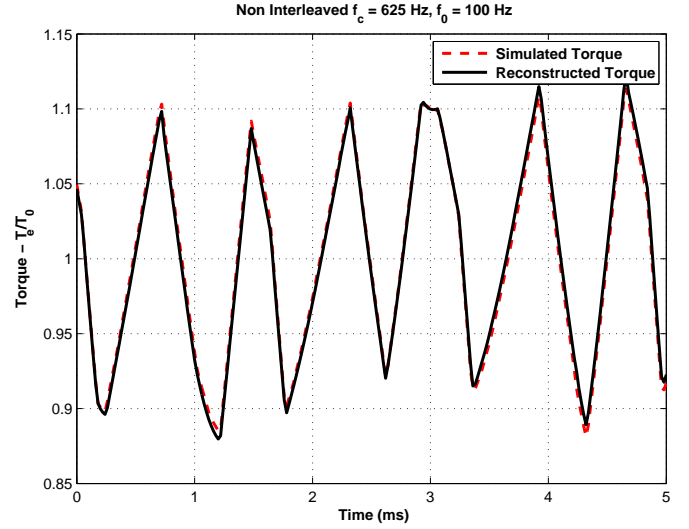


Fig. 13. Simulated and reconstructed airgap torque: no interleaved,  $f_c = 625$  Hz,  $f_0 = 100$  Hz

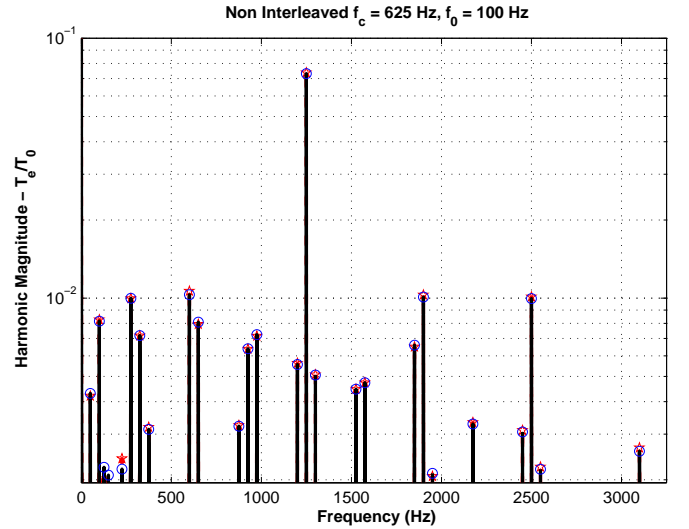


Fig. 14. Spectrum of the simulated (red dashed line with star markers) and reconstructed torque (black straight line with circle markers)

match between the simulated and the reconstructed torque can be achieved. This fact is further underlined by Fig. 14, which compares the spectra of these two torques.

## V. EXPERIMENTAL VALIDATION

For the experimental validation, the VSFS shown in Fig. 4 was built and tested extensively to power levels of up to 35 MW [13]. Hereafter, we show sample experimental results for the case of  $45^\circ$  interleaving. Fig. 15 shows the machine phase voltages and the stator currents. Based on the machine voltages and currents, the airgap torque was reconstructed, according to the method described and theoretically validated previously. The corresponding spectra of the phase current and the reconstructed torque are depicted in Fig. 16.

It should be noted that the reconstruction of the airgap torque as described in Section III-E was augmented by a post-processing step, in which a considerable second harmonic in

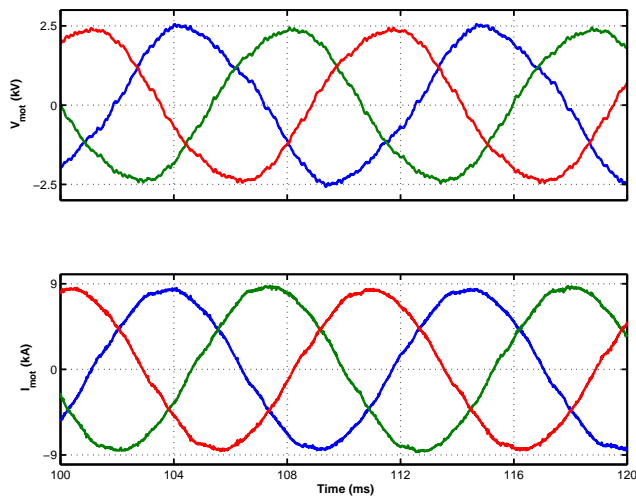


Fig. 15. Measured machine voltage (top) and current (bottom). The voltages and currents are (post processed) measured waveforms captured on a 35 MW VSDS

the reconstructed torque had to be removed. A preliminary analysis suggests that this harmonic at the frequency  $2f_0$  is due to measurement errors – specifically gain errors leading to three-phase currents and voltages of unequal fundamental amplitude and phase errors leading to phase shifts between the measured currents and voltages that are not exactly  $120^\circ$ . A detailed investigation of this issue is beyond the scope of this paper, but is planned for future work.

## VI. CONCLUSIONS

A method to predict possible operating points of PWM drives which may lead to physical damage of rotating shafts was presented. This approach combines the understanding of the propagation of the drive's airgap torque components on the shaft and the prediction of their location on the frequency axis. Simple and direct relationships between current harmonic frequencies and airgap torque frequencies were established, significantly reducing engineering efforts in the design stage. The proposed relationships can be easily extended to multi-level voltage source inverters and load commutated inverters, providing a useful approach to control engineers in order to avoid unwanted harmonic torque components and thus avoiding shaft excitation.

For some particular oil and gas system configurations such as high-speed integrated motor-compressor units, the motor is gas cooled making the measurement of the motor's airgap torque extremely challenging. Consequently, a method was proposed to reconstruct the airgap torque from the machine's line-to-line voltages and stator currents. This method is independent of the machine parameters and can be extended to other drive configuration.

Software simulations and experimental tests of four parallel connected IGCT-based 3-level NPC converters confirmed the accuracy of the suggested approaches.

## REFERENCES

[1] R. C. Quirt, *Voltages to ground in load-commutated inverters*, IEEE Trans. Ind. Applicat., vol. 24, no. 3, pp. 526-530, 1988.

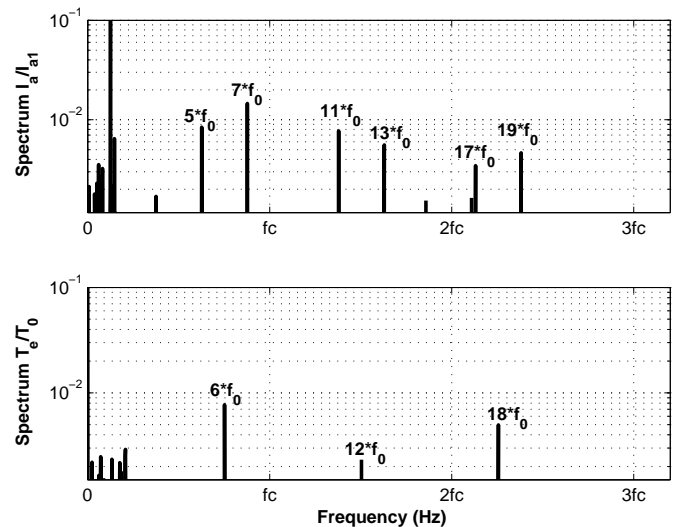


Fig. 16. Harmonic amplitude spectra of the measured machine current (top) and the reconstructed airgap torque (bottom)

- [2] F. A. Dewinter, L. G. Grainger, *A practical approach to solving large drive harmonic problems at the design stage*, IEEE Trans. Ind. Applicat. pp. 1095-1101, vol. 26, no. 6, Nov/Dec. 1990.
- [3] B. Wu and F. DeWinter, *Voltage stress on induction motors in medium-voltage PWM GTO CSI drives*, IEEE Trans. Power Electron., vol. 12, pp. 213-220, Mar. 1997.
- [4] M. Groetzbach, R. Redmann, *Line current harmonics of VSI fed adjustable-speed drives*, IEEE Trans. Ind. Applicat. pp. 683-690, vol. 36, no. 2, Mar./Apr. 2000.
- [5] J. Rodriguez, L. Moran, J. Pontt, R. Osorio and S. Kouro, *Modeling and analysis of common-mode voltages generated in medium voltage PWM-CSI drives*, IEEE Trans. Power Electron., vol. 18, no. 3, May 2003.
- [6] B.-T. Ooi, G. Joos, *The interaction of torsional resonances with network resonances in synchronous generators*, IEEE Trans. on Power App. and Sys., vol. PAS-104, no. 6, pp. 1426-1432, Jun. 1985.
- [7] C. Meckel, *Mechanical damage of a subsynchronous cascade drive due to torsional resonance*, Cement Industry Technical Conf., IEEE IAS/PCA, pp. 133-150, 2001.
- [8] C. Michael, A. Safacas, *Resonance effects in the electromechanical system of a tissue paper machine*, Int. Conf. on Electrical Machines and Systems, ICEMS, vol. 3, pp. 1907-1912, 2005.
- [9] J. Song-Manguelle, C. Sihler, J. M. Nyobe-Yome, *Modeling of torsional resonances for multi-megawatt drives design*, IEEE IAS 43rd Annual Meeting, Oct. 2008, Edmonton, Canada.
- [10] J. Song-Manguelle, J. M. Nyobe-Yome, *Pulsating torques in PWM multi-megawatt drives for torsional analysis of large shafts*, IEEE IAS 43rd Annual Meeting, Oct. 2008, Edmonton, Canada.
- [11] Du Zhong, L.M Tolbert, J. N. Chiasson, *Active harmonic elimination for multilevel converters*, IEEE Trans. on Power Elect., vol. 21, no. 2, pp. 459-469, March 2006.
- [12] R. Baccani, R. Zhang, et al., *Electric system for high power compressor trains in oil and gas applications - System design, Validation approach and performance*, Proc. 36th Turbomach. Symp., Texas A&M Univ., College Station, TX, 2007
- [13] S. Schröder, P. Tenca, et al., *Modular high-power shunt-interleaved drive system: a realization up to 35 MW for Oil & Gas applications*, IEEE IAS 43rd annual meeting, Oct. 2008, Edmonton, Canada.
- [14] C. Mung-Ong, *Dynamic Simulation of Electric Machinery using Matlab/Simulink*, Prentice hall, Purdue, 1999.
- [15] N. Piskounov, *Calcul différentiel et intal*, Ed. Mir, Moscow, 1971.
- [16] T. D. Graybeal *The nature of vibration in electric machinery*, Trans. of the Amer. Inst. Elect. Eng. Appl. Vol. 62, no 10, pp 712-718 Oct. 1944.
- [17] D. Walker, *Torsional vibration of turbomachinery*, McGraw-Hill, 2004.
- [18] T. A. Lipo, P. C. Krause, M. Hilscher *Stability Analysis of a Rectifier-Inverter Induction Motor Drive*, IEEE Trans. on Power Apparatus and Sys. Vol. 88, January 1969, pp. 55-66.
- [19] T. Feese, R. Maxfield, M. Hilscher *Torsional vibration problem with motor/ID fan system due to PWM variable frequency drive*, Proc. 37th Turbomach. Symp., Texas A&M Univ., College Station, TX, 2008.

- [20] R. Kerkman, J. Theisen, K. Shah *PWM inverters producing torsional components in ac motors*, IEEE-PCIC, Petroleum and Chemical Industr. Committee Techn. Conf, Cincinnati, OH, Sept. 2008.
- [21] C. Sihler, S. Schramm, J. Song-Manguelle, P. Rotondo, S. Del Puglia, E. Larsen, *Torsional Mode Damping for Electrically Driven Gas Compression Trains in Extended Variable Speed Operation*, Proc. 38th Turbomach. Symp., Texas A&M Univ., College Station, TX, 2009.
- [22] D. G. Holmes, B. P. McGrath, *Opportunities for harmonic cancellation with carrier-based PWM for two-level and multilevel cascaded inverters*, IEEE Trans. on Ind. Applicat., vol. 37, no. 2, pp 574-582, Mar./Apr. 2001.
- [23] D. G. Holmes, T. A. Lipo, *Pulse width modulation for power converters: principle and practice*, IEEE Press, Series on Power Eng., Wiley Interscience, 2003.
- [24] P. C. Krauze, O. Wasynczuk, S. C. Sudhoff *Analysis of electric machinery and drive systems*, 2nd Ed. IEEE press series on power engineering, Wiley-Interscience, 2002.
- [25] J. Holtz, J. Quan *Drift and parameter compensated flux estimator for persistent zero frequency operation of sensorless controlled induction motors*, IEEE Trans. on Ind. Appl. Vol. 39, no 4, pp 1052-1060 July/Aug. 2003.



**J. Song-Manguelle** (M'07, SM'10) was born in Makak, Cameroon. He received the B.S. and M.S. degrees in pedagogical sciences and electrical engineering from the University of Douala, Cameroon in 1995 and 1997, and a Ph.D. degree in electrical engineering from the Swiss Federal Institute of Technology (EPFL), Lausanne, Switzerland in 2004.

From 1997 to 1999, he was a lecturer at the University of Douala. In 1999, he joined the Industrial Electronics Lab. at EPFL as a post-graduate assistant, and from 2001 to 2004 he was a Research Associate and PhD candidate in the same institution.

In 2004, he joined GE Global Research Center, Munich, Germany, dealing with high-power drives topologies and control for various applications. From 2006 to 2007, he was with Thermodyn, a GE oil and gas business in Le Creusot, France as a Senior Electrical Engineer and Team Leader, dealing with high-power drives acquisition and torsional issues in compressor drive trains. From 2007 to 2008, he joined Baldor Electric, Montreal, Canada as a Senior Design Engineer. He spent part of his time with the Baldor Drives Center, Fort Smith, AR, focused on low-voltage high-power re-generative drives.

Since 2008, he is with GE Global Research Center, Niskayuna, NY. His areas of interest are topologies and control of high-power electronics, as well as large scale integrated electro-mechanical systems.



**S. Schröder** (S'98-M'03) received the Diploma and Ph.D. degrees in electrical engineering from RWTH Aachen University, Aachen, Germany, in 1997 and 2003, respectively. From 1997 to 2002, he has a Research Associate at the Institute for Power Electronics and Electrical Drives (ISEA), RWTH Aachen University, where he was working on power electronic circuits and devices in particular on high-power semiconductors. From July 2002 to December 2005, he was Chief Engineer at the same institute responsible for the research in the fields of electrical

drives, power electronic circuits, and semiconductor devices.

Since the beginning of 2005, he has been with GE Global Research Europe, Munich, Germany, where he is working on power electronic applications with focus on high-power converters for medium-voltage drives. He has authored or coauthored over 30 published technical papers. Dr. Schröder is a member of the German Association for Electrical, Electronic and Information Technologies (VDE).

He is a recipient of the 2009 second Prize Paper Award of the IEEE Transactions on Industry Applications.



**T. Geyer** (M'08) received his Dipl.-Ing. and Ph.D. degrees in Electrical Engineering from ETH Zurich, Switzerland, in 2000 and 2005, respectively. From 2006 to 2008, he was with GE's Global Research Center in Munich, Germany, where he was a project leader working on control and modulation schemes for large medium-voltage electrical drives. In late 2008 he joined the Power Electronics Group of the University of Auckland, New Zealand, as a Research Fellow. His research interests are at the intersection of modern control theory, optimization and power electronics, including model predictive control, hybrid systems, electrical drives and dc-dc conversion.

He is a recipient of the 2009 second Prize Paper Award of the IEEE Transactions on Industry Applications.



**J.M. Nyobe-Yome** was born in Yaoundé, Cameroon. He received a diploma of technical high-school teaching from the University of Douala-ENSET, Cameroon, a M.S degree from Ecole Normale Supérieure de Cachan and Université de Paris VI, France and a Ph.D. from Université de Montpellier II (STL), Montpellier, France respectively in 1984, 1986 and 1993 all in Electrical Engineering.

In 1985 he joined the University of Douala-ENSET as a lecturer, where he is now an Associate Professor. He is also head of the electrical engineering department and head of the industrial electronics and systems laboratory.

Since 1994, He has supervised more than 200 Master thesis in electrical engineering sponsored by local companies and the cameroonian government. He is a senior member of the cameroonian commission for technical education.

His areas of interest are resonant power conversion, high-power variable speed drives, wind-mill/diesel twinning and applied pedagogical sciences to electrical engineering.



**G. Ekemb** was born in Matomb, Cameroon. He received a B.S, M.S degrees in pedagogical sciences and electrical engineering, as well as a DEA in electrical engineering from the university of Douala-ENSET, Douala, Cameroon respectively in 1995, 1997 and 2006.

From 1997 to 2003, he was a teacher at the technical high-school of Nkongsamba, Cameroon. Since 2003, he joined the industrial electronics and systems laboratory, university of Douala-ENSET as a senior research associate, where is also working

toward his Ph.D, a collaboration with the University of Quebec, Rouyn-Noranda, QC, Canada.

His areas of interest are high-power conversion, electro-mechanical interactions and renewable energy power conversion.